Anomalous Dynamic Light Scattering from Solutions of Light Absorbing Polymers

Amit Sehgal and Thomas A. P. Seery*

Polymer Program and Department of Chemistry, University of Connecticut, Storrs, Connecticut 06269

Received March 2, 1999; Revised Manuscript Received September 13, 1999

ABSTRACT: Dynamic light scattering data from highly absorbing solutions exhibit intensity−intensity correlation functions characterized by a sum of exponential decays superposed with an oscillatory term. A new analytical treatment is proposed, which explains this behavior as arising from the heterodyning of scattered light from two distinct species in convective motion. Similar data were obtained both for solutions of polyaniline (PANI) as well as for a complex of cytochrome *c* and cytochrome *c* peroxidase in phosphate buffer. This suggests the generality of the phenomenon for polymers that both absorb light and aggregate, such as proteins and conducting polymers. Effects of laser power on convection, thermal lensing, and coning of the beam and concentration of absorbing species have been considered. The presence or absence of the oscillations is shown to be a sensitive indication of aggregation.

Introduction

Scattered light from polymeric solutions provides a wealth of information on the structure and motions of macromolecules, chain conformations and sizes, polymer−polymer and polymer−solvent interactions, and chain dynamics. Dynamic light scattering (DLS) in particular is capable of obtaining the distribution of sizes in a polymer solution. Therefore, it would be valuable to apply DLS to the characterization of polymers, where the extent of aggregation is an important factor in processing and function.

Conducting polymers, like polyanilines, are difficult to characterize by light scattering because solutions of conducting polymers typically absorb light.[1−4] Conjugation, which leads to conduction in polymers, is also responsible for the high absorptivity of solutions of the emeraldine base (EB), the emeraldine salt (ES), and the pernigraniline (PE) form of PANI. This leads to immense complications in data acquisition and analysis. In a light scattering experiment, where absorbing species are the object, the accessible concentration range is severely restricted by the need to minimize absorption (favoring low concentration) and maximize scattering (requiring high concentration). Besides restricting the concentration range accessible to the experiment, thermal lensing causes changes in the spatial power density of the laser beam. Temperature gradients result from this lensing and drive convective transport in the scattering volume.

While the complications arising from light absorption have been sufficient to deter most potential light scattering studies of highly conjugated molecules, a few examples can be found. Cotts et al. have successfully carried out DLS measurements on modified poly(phenyleneethynylenes), which have a greater solubility in common solvents, have no evidence of aggregation, and have far lower absorptivities in the visible region at the probing laser wavelengths.[5] Polarized and depolarized dynamic light scattering on regioregular dilute solutions of poly(dodecylthiophenes)[6] among other conjugated systems have also been reported.[7]

Static light scattering experiments on the emeraldine base of polyaniline in solution have shown the negative second virial coefficient to be an indicator of aggregation.[8,9] The weight-average molecular weight calculated from these experiments was grossly out of proportion with the GPC results.[9] This observation was attributed to thermal fluctuations in the solution. Further attempts to obtain molecular weight data for PANI have focused on the colorless leucoemeraldine form that may be synthesized directly or reduced in situ.[10] Comparison of those results with GPC suggested that chain scission due to the hydrazine used for reduction could be a limitation for this approach. Gettinger and Heeger[11] reported static light scattering data on EB−PANI with camphorsulfonic acid in *m*-cresol. The negative excess scattering intensities, even after correcting for absorption, from this highly conjugated system precluded any form of physical interpretation of the data. They also reported DLS data on the effect of excess water and polymer concentration in the system despite having great problems with sample stability. They attribute the second relaxation to large PANI aggregates convecting through the scattering volume. These observations and the potential utility of PANI as a processable conducting component in electronics packaging prompted us to attempt a dynamic light scattering study on EB−PANI.

Light scattering has also been used previously to characterize proteins that have similar characteristics to PANI, in that they absorb light in the visible range.[12,13] Proteins such as elastin[13] and cytochrome *c* exhibit aggregation phenomena similar to the behavior of conjugated polymers. In addition, Hall and co-workers have conducted a careful study on strongly absorbing and concentrated solutions of unliganded hemoglobin.[14] They considered effects such as convection, thermal gradients, and thermal lensing that would be typical sources of error. Though the effects of temperature gradients due to the laser were significant, convection and lensing in the scattering volume had minimal impact on their measurements. They do however suggest that the time scales of diffusion of the proteins are too small, as compared to the slower convective motions, to pick up any oscillatory behavior due to convection in the heterodyne geometry.

A homodyne scattering experiment cannot distinguish between random diffusion and diffusion with a constant

10.1021/ma9903106 CCC: $18.00
Published on Web 10/19/1999

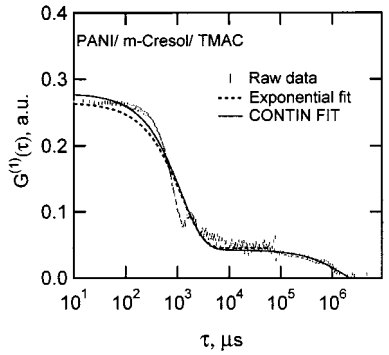

Figure 1. Typical correlation function for PANI in *m*-cresol with tetramethylammonium chloride (TMAC). Curves drawn from fits using CONTIN or a single exponential do not account for all features of the data; the data decay faster than the single exponential. [C_P = 0.0467 mg/mL; C_S = 16.67 mg/mL; T = 30 °C; θ = 40°.]

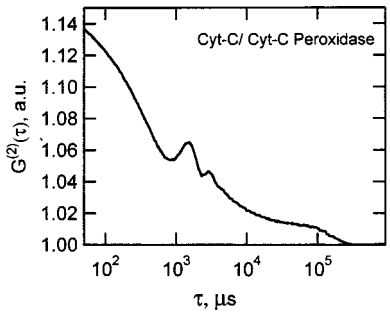

Figure 2. Oscillatory correlation functions from cyt-C/cyt-C peroxidase complex in phosphate buffer [pH = 7.0; $[PO_4]^{-4}$ = 60 mmol; θ = 25°; T = 30 °C]. This absorbing and aggregating protein has correlations similar to PANI.

velocity superposed on the random motion.[15] However, in laser doppler velocimetry flow profiles are mapped using heterodyne scattering.[16] Correlation of the scattered beam with the incident beam preserves information on the velocity of the macromolecules. Heterodyne light scattering has also been used in conjunction with electrophoresis[17,18] and sedimentation experiments[19] to observe the effects of an external field. The flow field results in a peak in the power spectrum of the scattered light or a periodic correlation function.[17−19] In our scattering experiments on absorbing systems, the incident beam is not mixed with the scattered beam, therefore our observations of periodic correlation functions are anomalous (Figure 1). This led us to reevaluate our data on highly absorbing solutions of associating polymers. A widely separated bidisperse population of scatterers can produce heterodyning effects where the "incident beam" is provided by scattering from the larger species. In this case an external velocity field results in periodic correlation functions.

The combination of light absorption and aggregation is also seen in a protein complex of cytochrome *c* and cytochrome *c* peroxidase. This heme protein absorbs strongly in the visible range, and in the absence of a stabilizer such as dithiothreitol, it will aggregate over time by forming disulfide bonds. DLS from this protein in solution exhibits oscillatory correlation functions (Figure 2), that are comparable to those seen in the PANI system. Similar characteristic correlations in two totally different systems with the same inherent absorbing and aggregating characteristics reflect on the generality of the phenomenon and support our explanation for it.

Experimental Section

Instrumentation. The DLS measurements were made with a Brookhaven Instruments BI9000-AT autocorrelator with a maximum of 356 data channels that permit simultaneous data acquisition and measurement of relaxation times from 0.025 μs to 10 s. A water-cooled Coherent Innova 70-3 argon ion CW laser was used for the experiment. The laser was tuned to its 488 nm line or the 514.5 nm line to maximize the amplitude of the observed correlation functions.

For these experiments, the laser power ranged from 200 mW to 1 W in the light control mode. The samples were prepared in 13 mm cylindrical scattering cells that were cleaned with condensing acetone vapor to remove dust. During measurements, the cells were thermostated in a decalin bath mounted on a Brookhaven BI200SM goniometer that enables automated measurements over the entire range of angles from 20 to 150°. For most of the following experiments, lack of sufficient scattered intensity restricted the useful range of angles to 20−60°. The temperature of the decalin bath is maintained by surrounding jackets and coils in a closed loop water circulation with a refrigerated temperature bath. An internal PID control maintains the bath temperature to within 0.01 °C of the set point.

Sample Preparation. The polyaniline was provided by Marie Angelopoulos of the IBM T. J. Watson research center, as filtered *N*-methylpyrrolidone (NMP) solutions and in the powder form. NMP solutions were diluted down from 0.1% stock solutions to nominal concentrations of 0.05 and 0.08 mg/mL in scintillation vials. The samples were subsequently used without further treatment. Solutions were considered "dust free" if no spikes in the average intensity were observed over the course of an experiment. The repeatability of the measurements over a 3-day period was a further criterion for clean solutions.

The *m*-cresol solutions were prepared from PANI in the dry powder form. Spectrophotometric grade *m*-cresol from Aldrich was used. Camphorsulfonic acid (CSA) and tetramethylammonium chloride (TMAC) were used to control doping and the ionic strength of the solution due to their high solubility in *m*-cresol. The TMAC is highly hygroscopic and was baked in an oven at approximately 200 °C for 30 min prior to use. An aliquot of a 25 mg/mL stock made from this dry crystalline salt was added to a previously prepared PANI solution to give the PANI/*m*-cresol/TMAC sample (C_p = 0.0455 mg/mL; C_{TMAC} = 16.67 mg/mL). The CSA sample was similarly prepared by mixing stocks to yield a PANI/*m*-cresol/CSA solution with a similar polymer concentration. (C_p = 0.05 mg/mL; C_{CSA} = 0.041 mg/mL). The *m*-cresol solutions were all filtered through a 1 μm PTFE, 25 mm cartridge filter into dust-free scattering cells.

Experiments were also carried out on cytochrome *c* peroxidase (provided by Gerard Jensen) and the cofactor cytochrome *c* (cyt-C). The cyt-C (M_w = 12 384 g/mol), a water-soluble protein derived from horse heart, was coupled with yeast cyt-C peroxidase (M_w = 33419 g/mol) in a 60 mmol potassium phosphate buffer (pH 7.0). The deep red solution of the protein complex was diluted with deionized water to a cyt-C concentration of 0.8 mg/mL. The solution was then filtered through a 0.2 μm PVDF filter (13 mm, Gelman Acrodisc) into the scattering cell. The sample was allowed to sit for several days before attempting data acquisition. The protein and its cofactor are known to form either a 1:1 or a 1:2 complex. The exact composition is a matter of some controversy[20,21] and was the initial subject for our study. Large aggregates without specific biological function are known to form over time via the disulfide bond formation.

Data Analysis. The intensity−intensity correlation functions obtained as the raw DLS data are related to the field correlation function $G^{(1)}(\tau)$ by the Seigert relationship:

$$G^{(2)}(\tau) = \langle I(0)\, I(\tau)\rangle = A(1 + \beta|G^{(1)}(\tau)|^2) \qquad (1)$$

In purely diffusive phenomena the field correlation function can be analyzed as of a spectrum of exponential decays:

$$G^{(1)}(t) = \int_0^\infty s(\tau)\, e^{-t/\tau}\, d\tau \quad (2)$$

Under normal circumstances the correlation functions are deconvoluted using Provencher's CONTIN, a constrained regularization method for inverting the Laplace transform, to yield the amplitudes $s(\tau)$.[22,23] Relaxation times are obtained from the average position of the peaks in these amplitude plots and are used to calculate the diffusion coefficients and hydrodynamic radii using the Stokes−Einstein relationship. Our data, in this case, show a faster than exponential decay with a periodic function overlaid on a slowly decaying tail. This cannot be represented by eq 2**,** so we have derived a model (vide infra) where the physics give rise to an oscillatory component. The data are fit to this functional form by an iterative process that minimizes the χ^2 value for the fit as compared to the raw data. This routine uses the Levenberg−Marquardt algorithm in a commercially available package to predict the value of the coefficients on every iteration and minimize χ^2.

Theory

Derivation of an Intensity−Intensity Correlation Function for Scattering from A Mixture of Two Distinct Species with Convective Motion. For a solution constituted of two mutually distinct diffusing species, e.g., aggregates and single chains, the field correlation function can be written as[15]

$$F_1(\mathbf{q},t) = \langle N_1\rangle\langle e^{i\mathbf{q}\cdot(\mathbf{r_1}(t) - \mathbf{r_1}(0))}\rangle + \langle N_2\rangle\langle e^{i\mathbf{q}\cdot(\mathbf{r_2}(t) - \mathbf{r_2}(0))}\rangle \quad (3)$$

or

$$F_1(\mathbf{q},t) = \langle N_1\rangle F_{S1}(\mathbf{q},t) + \langle N_2\rangle F_{S2}(\mathbf{q},t) \quad (4)$$

where F_{S1} and F_{S2} are the self-intermediate scattering functions for single chains and aggregates, respectively.

Illumination of solutions that have substantial absorption coefficients results in a temperature gradient that drives convective motion. In the case of a uniform velocity superposed on random fluctuations, the flux is[15]

$$\mathbf{J} = \mathbf{v}\cdot C(\mathbf{r},t) - D\cdot\nabla C(\mathbf{r},t) \quad (5)$$

Convective motion accelerates the molecules and the resulting velocity profile in the scattering cell will determine the macromolecular motion in solution. Combining the continuity equation with the equation for the flux, we get

$$\frac{\partial C(\mathbf{r},t)}{\partial t} + \mathbf{v}\cdot\nabla C(\mathbf{r},t) = D\cdot\nabla^2 C(\mathbf{r},t) \quad (6)$$

for constant velocity, $\mathbf{v}$, and diffusion coefficient, D.

The concentration, $C(\mathbf{r},t)$, is related to the self-intermediate scattering function, $F_s(\mathbf{q},t)$, through a Fourier transform. Fourier transformation and solution of the equations, subject to boundary condition of the probability at $t = 0$ being 1, yields

$$F_s(\mathbf{q},t) = e^{[i(\mathbf{q}\cdot\mathbf{v})t - \mathbf{q}^2 Dt]} \quad (7)$$

Since the macromolecules are not infinitely small, the velocity gradients in solution will exert a resultant intrinsic hydrodynamic force[24] due to shear that will depend on the size and the shape of the molecules. Because of this gradient, the drag on larger sized macromolecules should be greater than the drag on smaller counterparts, resulting in a velocity differential. This effect was first proposed by Segre and Silberberg[25] and is now used extensively in field flow fractionation (FFF).[26] Contributions of large and small scatterers can be added to form the total field correlation function as indicated by eq 4:

$$F_1(\mathbf{q},t) = \langle N_1\rangle e^{[i(\mathbf{q}\cdot\mathbf{v}_1)t - \mathbf{q}^2 D_1 t]} + \langle N_2\rangle e^{[i(\mathbf{q}\cdot\mathbf{v}_2)t - \mathbf{q}^2 D_2 t]} \quad (8)$$

The observed quantity in dynamic light scattering is the intensity−intensity autocorrelation function which is defined as

$$F_2(\mathbf{q},t) = \langle N_1 + N_2\rangle^2 + \langle\sum_j b_j(0)e^{-i\mathbf{q}\cdot\Delta\mathbf{r}_j(t)}\rangle\langle\sum_k b_k(0)e^{-i\mathbf{q}\cdot\Delta\mathbf{r}_k(t)}\rangle$$
$$= \langle N_1 + N_2\rangle^2 + F_1(\mathbf{q},t)\times F_1^*(\mathbf{q},t) \quad (9)$$

To obtain the intensity autocorrelation function, $F_1(\mathbf{q},t)$ is multiplied by its complex conjugate:

$$F_1(\mathbf{q},t)\times F_1^*(\mathbf{q},t) = \langle N_1\rangle^2 e^{-2\mathbf{q}^2 D_1 t} + \langle N_2\rangle^2 e^{-2\mathbf{q}^2 D_2 t} + \langle N_1\rangle\langle N_2\rangle e^{-\mathbf{q}^2(D_1+D_2)t}[e^{i\mathbf{q}\cdot(\mathbf{v_1}-\mathbf{v_2})t} - e^{-i\mathbf{q}\cdot(\mathbf{v_1}-\mathbf{v_2})t}] \quad (10)$$

which is equivalent to

$$F_1(\mathbf{q},t)\times F_1^*(\mathbf{q},t) = \langle N_1\rangle^2\, e^{-2\mathbf{q}^2 D_1 t} + \langle N_2\rangle^2\, e^{-2\mathbf{q}^2 D_2 t} + 2\langle N_1\rangle\langle N_2\rangle e^{-\mathbf{q}^2(D_1+D_2)t}\cos(\mathbf{q}\cdot\Delta\mathbf{v}\, t) \quad (11)$$

and gives the final result of the measured intensity−intensity correlation function

$$F_2(\mathbf{q},t) = \langle N_1 + N_2\rangle^2 + \langle N_1\rangle^2 e^{-2\mathbf{q}^2 D_1 t} + \langle N_2\rangle^2 e^{-2\mathbf{q}^2 D_2 t} + 2\cdot\langle N_1\rangle\langle N_2\rangle e^{-\mathbf{q}^2(D_1+D_2)t}\cos(\mathbf{q}\cdot\Delta\mathbf{v}\, t) \quad (12)$$

This model provides a term with a cosine function superposed on the expected double exponential decay. Convective motion, represented by the cosine function, is normally not observed in *homodyne* experiments for single scatterers.[15] The contribution of the complex part of $F_s(\mathbf{q},t)$ in eq 7 that contains this information disappears when multiplied by its conjugate as in eq 10. The measured intensity correlations in the homodyne mode therefore only show the diffusive component of the motion. However, the presence of the aggregates in our system fortuitously introduces the cross-multiplied terms that give us the measure of the relative velocity between the two convecting species. This has been shown above to be theoretically possible and is substantiated by our observations as discussed below. This effect can also be interpreted as a heterodyning effect and suggests that uniform motion can be measured even in the homodyne mode provided that very small amounts of another nonperturbing probe molecule are present.

Thermal Lensing and The Modified Scattering Vectors. Hall et al.[14] have made dynamic light scattering measurements on hemoglobin solutions, which, like polyaniline, absorb light. The absorption of light results in local heating of the solution. The effects of heating include thermal expansion that results in a decrease in the density and refractive index of the solution. The decrease in density causes the solution in the illuminated volume to rise due to its increased buoyancy. This is the driving force for the convective flow described above. The change in refractive index has an additional effect of creating a "lens" in solution so that the illuminating beam is transformed from a cylindrical to a conical geometry. This effect is referred to as thermal lensing or coning. The net result is a spread in the angle between the incident and the scattered beam and requires a reevaluation of the definition of the scattering vector.

Using previous conventions,[14] the incident beam lies along the z axis (Figure 3), but due to "coning" the propagation vector $\mathbf{k}_i$, [$|\mathbf{k}_i| = (2\pi n)/\lambda$] diverges by an angle φ that sweeps through a range from 0 to Δ. The detector is in the $y-z$ plane along the $\mathbf{k}_s$ vector and makes an angle θ_s with the z axis. The projection of $\mathbf{k}_i$ on the xy plane makes the angle ϕ with the x axis. The scattering vector $\mathbf{q} = \mathbf{k}_i - \mathbf{k}_s$. This is averaged over a solid angle, $d\Omega = (\sin\psi\, d\phi)\, d\psi$ so as to encompass the entire cone. So Γ_{avg} is defined as

$$\Gamma_{avg} = \frac{\int D\mathbf{q}^2\, d\Omega}{\int d\Omega} = \frac{\int_0^\Delta\int_0^{2\pi}\Delta\mathbf{q}^2\sin\psi\, d\phi\, d\psi}{\int_0^\Delta\int_0^{2\pi}\sin\psi\, d\phi\, d\psi} \quad (13)$$

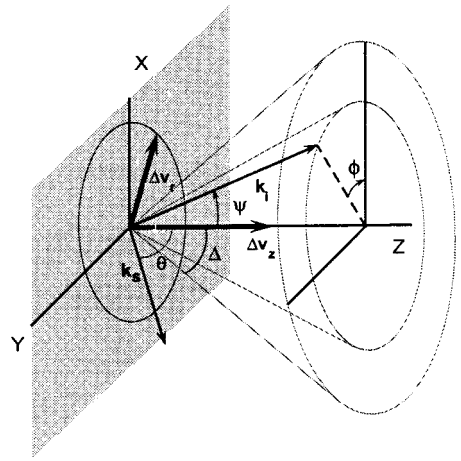

Figure 3. Coning geometry and symbol definitions.

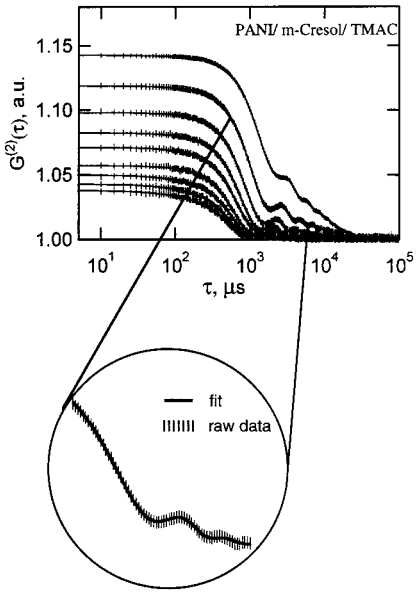

Figure 4. Correlation functions for angles from 20 to 60° in 5° increments for PANI in *m*-cresol with TMAC [$C_P = 0.0467$ mg/mL; $C_S = 16.67$ mg/mL; $T = 30$ °C].

Upon integration, the above formula yields a modified value of $\mathbf{q}^2$:

$$|\mathbf{q}|_{MOD}{}^2 = \left(\frac{4\pi n}{\lambda}\right)^2\left[\frac{1}{2}\left(1 - \frac{\cos\theta_s \sin^2\Delta}{2[1-\cos\Delta]}\right)\right] = \left(\frac{4\pi n}{\lambda}\right)^2\left[\frac{1}{2}\left(1 - \left(\cos\theta_s \cos^2\frac{\Delta}{2}\right)\right)\right] \quad (14)$$

In contrast, the usual definition of the scattering vector is

$$|\mathbf{q}|_{NORM}{}^2 = \left(\frac{4\pi n}{\lambda}\right)^2\left[\frac{1}{2}(1-\cos\theta_s)\right] = \left(\frac{4\pi n}{\lambda}\right)^2 \sin^2\left(\frac{\theta}{2}\right) \quad (15)$$

The $\cos\theta_s$ term in eq 14 is multiplied by $\cos^2(\Delta/2)$ with the result that

$$|\mathbf{q}|_{MOD}{}^2 > |\mathbf{q}|_{NORM}{}^2$$

The net effect of the modified $\mathbf{q}$ would be to give a positive intercept for a plot of Γ vs $\mathbf{q}_{NORM}{}^2$ at $\theta_s = 0$, as is observed in our experimental data (Figure 5). It follows from eq 13 and 14 that

$$\Gamma = D\cdot|\mathbf{q}|_{MOD^2} = C - C\alpha\cdot x \quad (16)$$

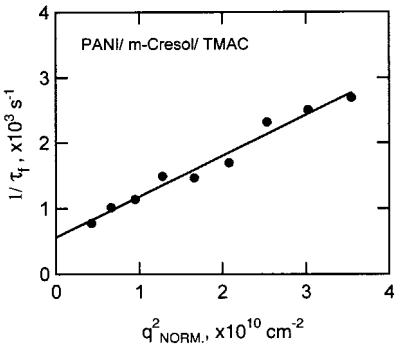

Figure 5. Inverse relaxation times against $\mathbf{q}^2$ for the fast relaxation. The slope provides $D^f_{app} = 3.11 \times 10^{-8}$ cm^2/s.

where

$$C = \frac{D}{2}\cdot\left(\frac{4\pi n}{\lambda}\right)^2; \quad \alpha = \cos^2\left(\frac{\Delta}{2}\right); \quad x = \cos\theta_s$$

Therefore, a plot of the inverse relaxation times (Γ) against $\cos\theta_s$ yields the value of D and the coning angle, Δ, as shown in Figure 6.

Referring back to the derived functional form of the correlation function (eq 12), it is evident that the period of the cosine term is also a function of the scattering vector, $\mathbf{q}$. The coning and the spread in $\mathbf{q}$ therefore necessitate averaging the product $\mathbf{q}\cdot\mathbf{v}$ over the same spatial coordinates. The velocity differential, $\Delta\mathbf{v}$, can be resolved into a radial and an axial component [$\Delta\mathbf{v} = \Delta\mathbf{v}_r + \Delta\mathbf{v}_z$]. The radial component, $\mathbf{v}_r$, can be further resolved into components that are parallel and perpendicular to the scattering plane. The cylindrical symmetry of the beam and the direction of the buoyant force determine the symmetry of the convective flow such that the components of $\mathbf{v}_r$ in the scattering plane cancel. Components of $\mathbf{v}_r$ that are perpendicular to the scattering plane have zero projection on $\mathbf{q}$, i.e., $\mathbf{q}\cdot\mathbf{v}_{r,\perp} = 0$. Therefore, the inverse time period for the oscillations is given by an integration over the surviving component, $\Delta\mathbf{v}_z$:

$$\frac{1}{\tau_v} = \frac{\langle\mathbf{q}\cdot\Delta\mathbf{v}\rangle}{2\pi} = \frac{1}{2\pi}\cdot\frac{\int\mathbf{q}\cdot\Delta\mathbf{v}\,d\Omega}{\int d\Omega} = \frac{1}{2\pi}\cdot\frac{\int_0^\Delta\int_0^{2\pi}\Delta\mathbf{v}_z\cdot(\mathbf{k}_i - \mathbf{k}_s)\cdot\sin\psi\,d\phi\,d\psi}{\int_0^\Delta\int_0^{2\pi}\sin\psi\,d\phi\,d\psi} \quad (17)$$

This yields

$$\frac{1}{\tau_v} = \frac{\Delta\mathbf{v}_z\cdot|\mathbf{k}_i|}{4\pi}\cdot\left(\frac{\cos^2\Delta}{1-\cos\Delta} - 2\cos\theta_s\right) = M\beta - 2Mx \quad (18)$$

where

$$M = \frac{\Delta\mathbf{v}_z\cdot n}{2\lambda}; \quad \beta = \frac{\cos^2\Delta}{1-\cos\Delta}; \quad x = \cos\theta_s$$

In Figure 7 and the discussion below, the plot of $\Gamma_{v,avg}$ against $\cos\theta_s$ is shown to be a straight line with a negative slope, which yields the value of the velocity differential along the z axis, $\Delta\mathbf{v}_z$, and also the coning angle, Δ. This procedure also gives us $|\mathbf{q}|_{MOD}$ which is distinct from $|\mathbf{q}|_{MOD}{}^2$:

$$|\mathbf{q}|_{MOD} = \left(\frac{2\pi n}{\lambda}\right)\cdot\left[\frac{1}{2}\left(\frac{\cos^2\Delta}{1-\cos\Delta} - 2\cos\theta_s\right)\right] \quad (19)$$

Results and Discussion

Polyaniline solutions were characterized in their highly absorbing emeraldine base and emeraldine salt

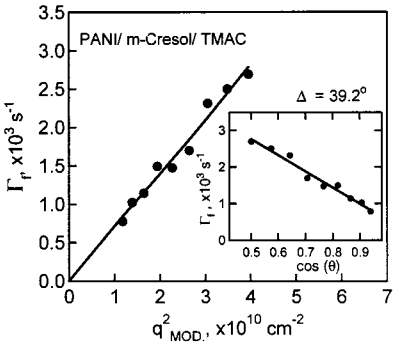

Figure 6. Relaxation times from fits to the data in Figure 4 plotted against the modified $\mathbf{q}^2$ vector. The coning angle of $\Delta = 39.2$ and the value of $D = 3.5 \times 10^{-8}$ cm^2 s^{-1} are calculated from the Γ_f vs cos θ_s plot (inset). [$C_P = 0.0467$ mg/mL; $C_S = 16.67$ mg/mL; $T = 30$ °C.]

forms in NMP and *m*-cresol by DLS. The unique nature of the correlations, characterized by a faster than exponential decay followed by an oscillatory tail, suggested the need to develop a new treatment to enable us to study these systems. The absorbing nature of the solutions and the aggregating characteristics of polyaniline pointed to the convection induced mobility of the macromolecules of two distinct average sizes as a possible model for explaining the data.

The primary observation in this work, autocorrelation functions with superposed oscillations, can be seen in Figure 4. These data were acquired from PANI solutions in *m*-cresol with added tetramethylammonium chloride at 30 °C ($C_p = 0.0467$ mg/mL; $C_s = 16.67$ mg/mL). The figure shows results from an angular scan from 20 to 60°. At higher angles, the data quality deteriorates rapidly. The normalized data was fit to a function similar to that derived above for the simultaneous diffusion and convection of two distinct species in solution (eq 20).

$$F(t) = 1 + w_0\, e^{-(t/w_1)} + w_2\, e^{-(t/w_3)} + w_4\, e^{-(t/w_5)} \cos(w_6 t + w_7) \quad (20)$$

This seven-parameter function was initially developed on a heuristic basis to fit the data seen in Figure 4. Inspection of the correlation functions clearly shows an initial decay between 10^2 and 10^3 μs. This motivates parameters w_0 and w_1 following the typical approach for analyzing DLS data. The second region of interest includes an oscillatory component with an extremely regular period and decaying amplitude. These features are incorporated using w_4 through w_7. The fact that the oscillatory region has a slope (this is most clearly seen for the correlation functions seen at the two lowest angles) motivates the incorporation of a second decay term that uses w_2 and w_3. This function provides excellent agreement with the data, but the inclusion of so many parameters begs the question of their value. Referring back to eq 12, two additional criteria will be used to demonstrate their relevance. eq 12 provides relationships between coefficients w_0, w_2, and w_4 and between relaxation times w_1, w_3, and w_5:

$$w_4 = 2\sqrt{w_0 w_2} \quad \text{and} \quad \frac{1}{w_5} = \frac{1}{2}\left(\frac{1}{w_1} + \frac{1}{w_3}\right) \quad (21)$$

Deviations from these relationships are within 50% for the majority of the data in Figure 4. Attempts to use these relationships to reduce the number of parameters did not converge well and gave inconsistent results with the second and more important criterion. The second criterion for validating these fitting parameters was their $\mathbf{q}$ dependencies.

It is important to recognize that the qualitative features of these data are uniquely dependent on, and therefore revealing of, the underlying physics. In fact, the oscillation itself is an indication of and an assay for the presence of aggregates. The amplitude of the oscillatory term is proportional to the product of the populations of the fast and the slow scatterers. Therefore, some population of each is required for observing oscillations. Furthermore, the observation of an oscillatory component in a correlation function that is, in all other respects, single exponential indicates the presence of a small population of larger scatterers that might otherwise escape detection. Filtration through a 0.2 μm filter removes the aggregates, making it difficult for time average intensity correlations to develop. Data acquired immediately after filtration were noisy and required averaging over long periods.

Comparing the fitting parameters to eq 12 derived for the bimodal model, w_1 and w_3 can be related to the diffusion coefficients, D^f_{app} and D^s_{app}, e.g.

$$\tau_f = w_1 = \frac{1}{2D^f_{app}\cdot\mathbf{q}^2} \quad (22)$$

Figure 5 is a plot of Γ_f ($=1/w_1$) vs $\mathbf{q}_{NORM}{}^2$, and the expected linear dependence is clearly seen. The apparent diffusion coefficient calculated from the slope of the line in Figure 5 is 3.11×10^{-8} cm^2 s^{-1}. However, it is clear that this analysis cannot be correct because the line in Figure 5 has a nonzero intercept. This observation stimulated efforts to compensate for the coning effect. Using eq 16, Γ_f is plotted against cos θ_s to obtain the coning angle, Δ, of 39.2°. Then $\mathbf{q}_{MOD}{}^2$ is calculated, and the plot of Γ_f vs $\mathbf{q}_{MOD}{}^2$ (Figure 6) is linear, but now with a zero intercept. The diffusion coefficient calculated from this plot is 3.5×10^{-8} cm^2 s^{-1}, or about 15% different from the analysis where coning is ignored.

The period of the oscillatory component (τ_v) calculated from the fit is related to the velocity differential (eq 23) through the scattering vector. In Figure 4 it is apparent that the period of the oscillation changes with angle. The values of the angular frequency "w_6" obtained from the fit to eq 20 were used to calculate the inverse period of oscillation that is identified with $\Delta\mathbf{v}_z$ in eq 17:

$$\frac{1}{\tau_v} = \frac{\langle \mathbf{q}\cdot\Delta\mathbf{v}_z\rangle}{2\pi} = \frac{w_6}{2\pi} \quad (23)$$

The period is plotted against the cosine of the scattering angle (cos θ_s) to calculate $\Delta\mathbf{v}_z$ from the slope as given by eq 18. Figure 7 shows the plot to be a straight line as predicted by the analytical treatment above. As pointed out earlier, the assumption of net radial convection perpendicular to the scattering plane precludes any contribution from the $\Delta\mathbf{v}_r$ component, making only the axial z component of the velocity differential ($\Delta\mathbf{v}_z$) visible to the experiment. The straight-line dependence supports the model of convective motion and the value of $\Delta\mathbf{v}_z = 0.0392$ cm s^{-1}. This is a reasonable value and agrees with the previously reported approximate observations.[11] The intercept of the straight line is a function of the coning angle, and yields $\Delta = 39.95°$. This

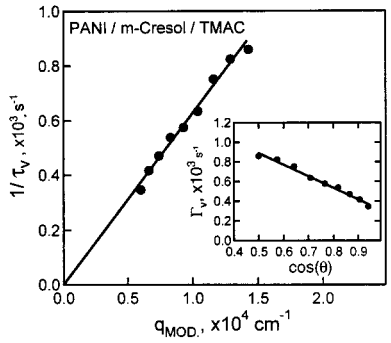

Figure 7. Inverse time period of the oscillations ($1/\tau_v$) fits to eq 20 the corrected scattering vector, $\mathbf{q}_{MOD}$. The velocity differential ($\Delta\mathbf{v}_{z,avg} = 0.0392$ cm s^{-1}) and the coning angle ($\Delta = 39.95°$) are calculated from the slope and the intercept of the $1/\tau_v$ vs cos θ_s plot. [$C_P = 0.0467$ mg/mL; $C_S = 16.67$ mg/mL; $T = 30$ °C.]

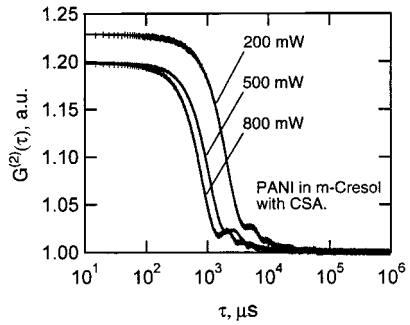

Figure 8. Correlations functions for PANI in *m*-cresol at fixed angle with increasing laser power. [$C_P = 0.05$ mg/mL; $C_S = 0.041$ mg/mL; $T = 30$ °C; $\theta = 40°$.]

independently corroborates the value of the coning angle ($\Delta = 39.2°$) obtained from the Γ_f vs cos θ_s plots.

The $\mathbf{q}^2$ dependence of the fast mode relaxation times and the $\mathbf{q}$ dependence of the frequency of oscillations, as shown by Figures 6 and 7, respectively, provide strong support for our model. However, the fitting procedure outlined by eq 20 yielded a constant phase angle, $w_7 = 3\pi/2$, in the periodic term. This constant angle persists for all samples under all experimental conditions. This phase shift no doubt lies in features of the physics not accounted for by our simple model that we have not been able to identify at present. This phase angle could possibly result from incorporating effects such as polydispersity for each of the diffusing species and warrants further investigation.

Effect of Laser Power. Given the premise that light absorption leads to local heating and convection, it is important to establish the dependence of these phenomena on the laser power. Dynamic light scattering data was obtained as a function of laser power from a solution of E−B PANI in *m*-cresol with added camphorsulfonic acid ($C_p = 0.05$ mg/mL; $C_s = 0.041$ mg/mL). Figure 8 shows correlation functions for this solution that were acquired at a 40° angle using laser powers of 200, 500, and 800 mW. This collection of data shows the effects of laser power. The initial decay and the first maximum in the correlation functions shift to faster times as the laser power increases. This translates to faster diffusion and faster convection respectively**.** Figure 9a is a plot of the fast diffusion coefficient extracted from the data in Figure 8 using eq 20 and correcting for coning. The velocity differentials, $\Delta\mathbf{v}$, are also taken from the fits; these are plotted against laser power in Figure 9b. The increased rate of diffusion probably results from the

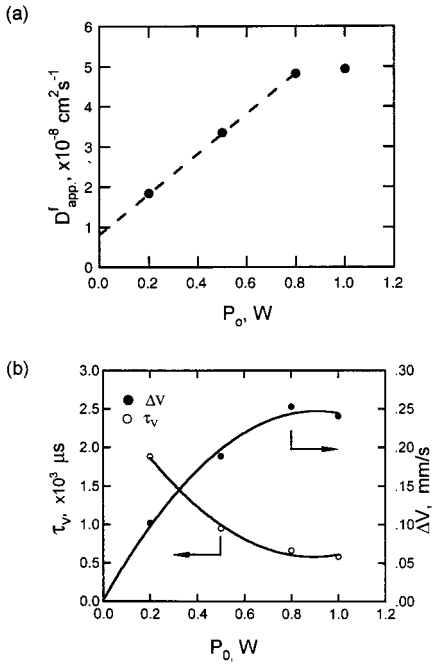

Figure 9. (a) Apparent diffusion coefficients, D^f, against laser power, P_0. $D^f(0) = 8.5 \times 10^{-9}$ cm^2 s^{-1}. (b) $\Delta\mathbf{v}_z$ against laser power. [$C_P = 0.05$ mg/mL; $C_S = 0.041$ mg/mL; $T = 30$ °C; $\theta = 40°$.]

decrease in solvent viscosity due to laser-induced heating of the solution. The increase in solvent quality that is normally expected from the rise in temperature would lead to chain expansion and give the opposite power dependence. This is a second-order effect and is probably not significant in this case. As seen in the correlation functions, the diffusion coefficients and velocities increase monotonically with input power. This supports the assumption that the laser heats the solution, driving convection. Data acquired at 1 W falls directly under the 800 mW curve (The 1 W data are not plotted in Figure 8). In Figure 9, this is shown by a corresponding leveling off in the diffusion coefficient and the $\Delta\mathbf{v}$ estimates at about 800 mW**.** As the laser power is increased, convection contributes to heat transfer from the scattering volume. The rise in temperature is not as great as would be predicted if absorption were considered alone. Therefore, the increase in the diffusion coefficients and convection velocities is lower than expected as laser intensity increases. In Figure 9a, the values at the three lowest laser powers are collinear and the line through them intersects the *y* axis at a finite value of 8.5×10^{-9} cm^2 s^{-1}. This corresponds to a hydrodynamic radius of 26 nm. This finite value is expected at zero power, where the laser no longer perturbs the system and thermal energy is sufficient for diffusive motion. On the other hand, $\Delta\mathbf{v}$ is completely a product of the laser-induced convection, and thus a quadratic fit to the $\Delta\mathbf{v}$ plotted in Figure 9b intersects the origin. These observations on the zero power values of D_f and $\Delta\mathbf{v}$ are consistent with physical assumptions of the model.

Effect of Concentration. The undoped EB−PANI in NMP is a deep blue solution that has a very limited range of concentrations available for data acquisition. Over most of the experimentally accessible concentration range the absorption of the beam is great enough that the beam cannot be seen to pass completely through the sample. The 488 nm Ar^+ line was used to

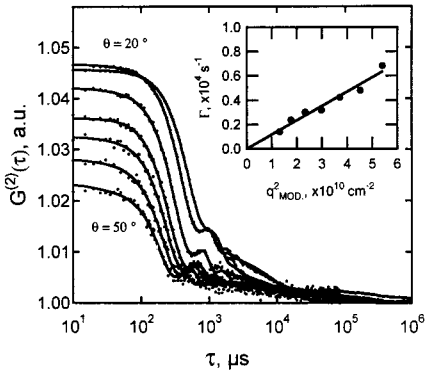

Figure 10. Correlation functions for EB−PANI in *N*-methyl pyrrolidone (NMP) over scattering angles from 20 to 50°. The fits to eq 20 are superposed on the raw data, and Γ_f is plotted against q_{MOD}^2. [C_P = 0.05 mg/mL; λ = 488 nm; T = 30 °C.]

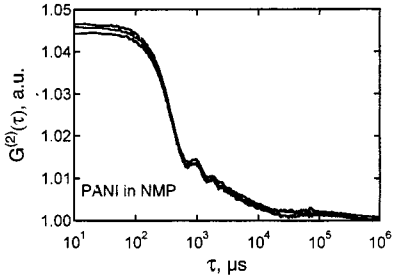

Figure 11. Three superposed correlation functions acquired with the laser power at 1 W over 3 days of continuous illumination. [C_P = 0.05 mg/mL; λ = 488 nm; T = 30 °C; θ = 25°.]

minimize absorption and maximize scattering. However, due to the attenuated scattering intensity, correlation could be achieved only by increasing the incident laser power to 1 W. The data (for C_p =0.05 mg/mL) showed the characteristic faster-than-exponential decay followed by the broad oscillatory tail (Figure 10). The correlations were fit to the derived expression (eq 12), and the relaxation times were plotted against the cosine of the scattering angle according to eq 16 giving D^f_{app} = 2.35 × 10^{-7} cm^2 s^{-1} and a coning angle Δ = 20°. The high laser power necessary for these experiments raises the question of degradation and thermal stability of the polymer under these conditions. Therefore, the sample was subjected to exposure to the laser at 1 W through three temperature cycles of 30−50−70 °C over a period of 3 days. The results were reproducible and showed no thermal or photodegradation (Figure 11).

A similar measurement was made for C_p = 0.08 mg/mL at 30 °C giving a fast mode diffusivity of 1.53 × 10^{-7} cm^2 s^{-1} and a coning angle of 34.95° in a similar plot of Γ_f against cos θ_s (Figure 12). This result is exceptional since it represents a large decrease in molecular mobility with a slight increase in concentration under the same apparent experimental conditions. The solutions are extremely dilute from the standpoint of chain overlap or excluded volume considerations; therefore, a 50% increase in diffusivity with a change from C_p = 0.08 to C_p = 0.05 mg/mL is unexpected. The explanation of this phenomenon depends on the spatial profile of absorption in the sample relative to the scattering volume. The increased absorption at higher polymer concentration will cause a steeper temperature profile, and this is evident, in part, in the observation of an increased coning angle. In other words the intensity of light reaching the scattering volume will be diminished

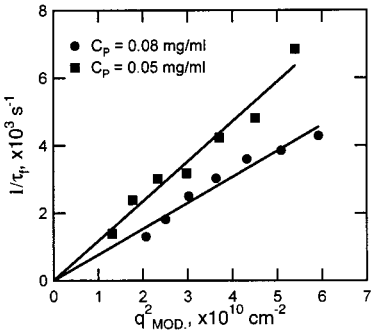

Figure 12. EB−PANI in NMP at C_P = 0.05 mg/mL (■), D_f = 2.35 × 10^{-7} cm^2 s^{-1}; and at C_P = 0.08 mg/mL (●), D_f = 1.53 × 10^{-7} cm^2 s^{-1}.

by the larger absorptivity of the higher concentration solution. The effective temperature at the scattering volume will therefore be lower because less light is absorbed at that point, giving rise to a higher local viscosity and reduced diffusion coefficients. This may seem contradictory if one considers that the higher concentration solution is better able to absorb light and therefore should experience greater heating. However, these solutions are in a concentration regime where effectively all of the laser power is absorbed and the important factor is the intensity seen by the scattering volume. The change in coning angle also lends support to this analysis. At lower concentrations, the smaller coning angle provides a more focused (or less defocused) beam so that a higher intensity illuminates the sample volume. Furthermore, the coning angle itself is increased at higher concentrations because a greater absorption of light at the entrance to the cell results in a better thermal lens.

These thermal effects mean that the temperature profile inside the solution is complex and that the density and the viscosity of the solution will be challenging to model in three dimensions. This complicates the process of extracting the hydrodynamic radius of a polymer from scattering data on absorbing solutions. One approach would be to extrapolate the diffusion coefficients to zero laser power. A more realistic method would be to use a latex sphere whose radius could be determined in the solvent in the presence and absence of light absorbing species. This experiment can be carried out in an absorbing medium with the same optical density as the absorbing polymer solution of interest so that the same amount of light is absorbed. The absorbing component of the model solution should be chosen to have the same optical characteristics as the polymer of interest, e.g., oligomers. In this way, the diffusion coefficient of the latex can be determined in the presence or absence of the thermal convection. Then the Stokes−Einstein relation will provide the ratio of temperature to solvent viscosity that is necessary to calculate the polymer radius from a measured diffusion coefficient.

Conclusions

Most light scattering experiments are performed on transparent solutions for good reasons. Solutions that absorb the incident light are subject to several problems that make the interpretation of light scattering data difficult. Absorption places an upper limit on the concentrations that may be studied by scattering. Absorption also heats the sample and that changes the temperature, density, refractive index, and viscosity.

These factors further lead to thermal lensing that changes the geometry of the experiment and a velocity field that perturbs motions of the macromolecules being observed. Nonetheless, there exist many light absorbing systems where an in situ technique for obtaining particle sizes is desirable, e.g., conducting polymers, proteins, and semiconductor quantum dots.

We have addressed these problems for systems that absorb light and aggregate. A simple model of scatterers with a bimodal size distribution in a convective flow field provides most of the features in the observed correlation functions. If the large and small scatterers in the model have unique velocities and diffusion coefficients then the relative velocity and the diffusion coefficients have the predicted dependencies on the scattering vector and are a function of laser power. The manner in which the large scatterers enter the model is such that the oscillations may be observed even when the concentration of aggregates is small. Therefore, the detection of an oscillatory component to the correlation functions is a sensitive indicator of the presence of aggregates. On the other hand, light scattering from larger objects is reduced at higher angles so that these phenomena will be seen primarily at lower angles. This approach will find general application in the study of both conducting polymers and proteins where light absorption is problematic and the extent of aggregation is an object of study. It would be of interest to develop model systems so that the interpretation of this model can be extended and particle sizes obtained quantitatively. Mixed solutions of polymers and solid spheres where the radii are separately determined and the solvent medium can be made to absorb light through the addition of absorbing species form the basis of future work.

Acknowledgment. The authors would like to thank Gerard Jensen of Nexstar Pharmaceuticals for the cytochrome *c* peroxidase and Marie Angelopoulos of IBM T. J. Watson Research Center for providing the PANI and for valuable discussions on PANI aggregation. Financial support for this work was provided in part by IBM.

References and Notes

(1) Stejskal, J.; Kratochvil, P.; Radhakrishnan, N. *Synth. Met.* **1993**, *61*, 225−231.
(2) Colomban, P.; Folch, S.; Gruger, A.; Regis, A.; Michel, D. *C. R. Acad. Sci. Ser. IIb: Mec. Phys., Chim., Astron.* **1996**, *322*, 63−70.
(3) Neoh, K. G.; Pun, M. Y.; Kang, E. T.; Tan, K. L. *Synth. Met.* **1995**, *73*, 209−215.
(4) Stejskal, J.; Kratochvil, P.; Jenkins, A. D. *Collect. Czech. Chem. Commun.* **1995**, *60*, 1747−1755.
(5) Cotts, P. M.; Swager, T. M.; Zhou, Q. *Macromolecules* **1996**, *29*, 7323−7328.
(6) Yue, S.; Berry, G. C.; Mccullough, R. D. *Macromolecules* **1996**, *29*, 933−939.
(7) Berry, G. C.; Cotts, P. M.; Chu, S.-G. *Br. Polym. J.* **1981**, *13*, 47−54.
(8) Stejskal, J.; Kratochvil, P.; Gospodinova, N.; Terlemezyan, L.; Mokreva, P. *Polymer* **1992**, *33*, 4857.
(9) Liao, Y. H.; Angelopoulos, M.; Levon, K. *J. Polym. Sci., Part A: Polym. Chem.* **1995**, *33*, 2725−2729.
(10) Hsu, C.-H.; Peacock, P. M.; FLippen, R. B.; Manohar, S. M.; MacDiarmid, A. G. *Synth. Met.* **1993**, *60*, 233−237.
(11) Gettinger, C. L.; Heeger, A. J.; Pine, D. J.; Cao, Y. *Synth. Met.* **1995**, *74*, 81−88.
(12) Roberts, J. L.; Conway, G. *Anal. Chim Acta* **1970**, *51*, 128−130.
(13) Jamieson, A. M.; C. E.; D.; Walton, A. G. *Biochim. Biophys. Acta* **1972**, *271*, 34−47.
(14) Hall, R. S.; Oh, Y. S.; Johnson, C. S. *J. Phys. Chem.* **1980**, *84*, 756−767.
(15) Berne, B. J.; Pecora, R. *Dynamic Light Scattering*; John Wiley & Sons: New York, 1976.
(16) Pike, E. R. In *Photon Correlation Spectroscopy and Velocimetry*; Cummins, H. Z., Pike, E. R., Eds.; Plenum: New York, 1977; pp 246−343.
(17) Ware, B. R.; Flygare, W. H. *Chem. Phys. Lett.* **1971**, *12*, 81−85.
(18) Ware, B. R.; Flygare, W. H. *J. Colloid Interface Sci.* **1972**, *39*, 670−675.
(19) Wada, A.; Nishio, I.; Soda, K. *Rev. Sci. Instrum.* **1979**, *50*, 458−463.
(20) Zhou, J. S.; Hoffman, B. M. *Science* **1994**, *265*, 1693−1696.
(21) Zhou, J. S.; Nocek, J. M.; DeVan, M. L.; Hoffman, B. M. *Science* **1995**, *269*, 204−207.
(22) Provencher, S. W. *Comput. Phys. Commun.* **1982**, *27*, 213.
(23) Provencher, S. W. *Comput. Phys. Commun.* **1982**, *27*, 229.
(24) Kononenko, V. L.; Shimkus, J. K. *J. Chromatogr.* **1990**, *520*, 271−285.
(25) Segre, G.; Silberberg, A. *J. Fluid Mech.* **1962**, *14*, 136−157.
(26) Giddings, J. C. *Science* **1993**, *260*, 1457−1465.

MA9903106